Title
TOPAS-nBio simulation of temperature-dependent indirect DNA strand break yields

Journal
Physics in Medicine and Biology, 67(14)

ISSN
0031-9155

Authors
Ramos-Méndez, José
García-García, Omar
Domínguez-Kondo, Jorge
et al.

Publication Date
2022-07-21

DOI
10.1088/1361-6560/ac79f9

Peer reviewed

HHS Public Access

Author manuscript

Phys Med Biol. Author manuscript; available in PMC 2023 July 08.

Published in final edited form as:

Phys Med Biol. ; 67(14): . doi:10.1088/1361-6560/ac79f9.

TOPAS-nBio simulation of temperature-dependent indirect DNA strand break yields

José Ramos-Méndez[1,*], **Omar García-García**[2], **Jorge Domínguez-Kondo**[2], **Jay A LaVerne**[3], **Jan Schuemann**[4], **Eduardo Moreno-Barbosa**[2], **Bruce Faddegon**[1]

[1]Department of Radiation Oncology, University of California San Francisco, San Francisco, California 94115, USA.

[2]Facultad de Ciencias Físico Matemáticas, Benemérita Universidad Autónoma de Puebla, Puebla, México 72000, MEX.

[3]Radiation Laboratory and Department of Physics, University of Notre Dame, Notre Dame, Indiana 46556, USA

[4]Physics Division, Department of Radiation Oncology, Massachusetts General Hospital & Harvard Medical School, Boston, MA, USA

Abstract

Current Monte Carlo simulations of DNA damage have been reported only at ambient temperature. The aim of this work is to use TOPAS-nBio to simulate the yields of DNA single-strand breaks (SSBs) and double-strand breaks (DSBs) produced in plasmids under low-LET irradiation incorporating the effect of the temperature changes in the environment.

A new feature was implemented in TOPAS-nBio to incorporate reaction rates used in the simulation of the chemical stage of water radiolysis as a function of temperature. The implemented feature was verified by simulating temperature-dependent G-values of chemical species in liquid water from 20 °C to 90 °C. For radiobiology applications, temperature dependent SSB and DSB yields were calculated from 0 °C to 42 °C, the range of available published measured data. For that, supercoiled DNA plasmids dissolved in aerated solutions containing EDTA irradiated by Cobalt-60 gamma-rays were simulated.

TOPAS-nBio well reproduced published temperature-dependent G-values in liquid water and the yields of SSB and DSB for the temperature range considered. For strand break simulations, the model shows that the yield of SSB and DSB increased linearly with the temperature at a rate of $(2.94\pm0.17)\times10^{-10}$ $Gy^{-1}Da^{-1}$ $°C^{-1}$ (R^2=0.99) and $(0.13\pm0.01)\times10^{-10}$ $Gy^{-1}Da^{-1}$ $°C^{-1}$ (R^2=0.99), respectively.

The extended capability of TOPAS-nBio is a complementary tool to simulate realistic conditions for a large range of environmental temperatures, allowing refined investigations of the biological effects of radiation.

[*]Corresponding author: Jose.RamosMendez@ucsf.edu.

1 Introduction

When cells are irradiated with low LET radiation (~0.3 keV/μm for ^{60}Co), the majority of DNA damages are induced not by the direct interactions of the radiation field with DNA, but by chemical reactions following radiolysis. Radiation chemistry is thus essential to understand the underlying mechanisms of the biological damage caused by ionizing radiation. Monte Carlo track-structure (MCTS) codes offer detailed simulations of particle tracks in media such as a cell. Several MCTS codes have further been developed with the capability to simulate the radiolysis of water and subsequent nonhomogeneous chemistry. Initial MCTS simulations used pure water as targets with overlayed DNA geometries to characterize physics interactions (Charlton 1986). Now, MCTS codes have become more sophisticated and can combine the physico-chemical processes of ionizing radiation with DNA geometry models.

MCTS has been used to quantify biological damage in the form of clustered single-strand breaks (SSB) and double-strand breaks (DSB) calculated at room temperature (Moiseenko et al 1998, Dingfelder *et al* 2008, Stepán and Davídková 2014, Nikjoo *et al* 2016, Friedland *et al* 2017, Lampe *et al* 2018, Schuemann *et al* 2019, Sakata *et al* 2019, Zhu *et al* 2020). However, temperature is well-known to impact the reaction kinetics that follow radiolysis (Elliot and Bartels 2009). Its effect in radiobiological measurements of SSB and DSB induced in plasmids and cells have been reported under different temperatures ranging from −20°C to 40°C (Tomita *et al* 1995a, Sahu *et al* 1997, Elmroth *et al* 2000). Temperature also impacts detecting techniques, for example, affecting the yield of SSB and DSB in gel electrophoresis (Jones *et al* 1994). While this effect is outside the capabilities of existing MCTS codes, they can be extended to predict the effect of temperature at the early times after irradiation, hence contributing further information to facilitate the analysis of measured DNA damages.

The success of MCTS codes relies on the fairly accurate reproduction of experimental conditions. The capability of MCTS codes to simulate the temperature dependence of radiolitic yields in water has been reported in the range of 25 °C – 700 °C (Hervé du Penhoat *et al* 2000, 2001, Kanike *et al* 2016, Sultana *et al* 2020, Plante 2011). However, to the best of our knowledge, no MCTS code has so far integrated temperature dependence for the estimation of SSB and DSB yields. To further improve the accuracy of MCTS predictions of DNA damage yields it is thus important to incorporate temperature-dependence capabilities in a modeling tool.

The approach to simulate the effect of temperature used by MCTS codes consists of scaling chemistry parameters (diffusion coefficients and reaction rate constants) as a function of the temperature relying on experimental measurements such as those compiled by Elliot et al. (Elliot 1994, Elliot and Bartels 2009). However, the availability of MCTS codes including temperature-dependence for the chemical stage is limited or restricted to laboratories where they were developed. The Geant4-DNA code is the first open-source MCTS (Incerti *et al* 2018a, Bernal *et al* 2015, Incerti *et al* 2010b, 2010a). However, a steep learning curve is needed to fully exploit the capabilities of that tool. To overcome this limitation, the radiobiological framework TOPAS-nBio, which wraps and extents Geant4-DNA, has been

developed to facilitate the implementation of MCTS simulations through a user-friendly interface (Schuemann *et al* 2019). In this work, we report an extension of TOPAS-nBio that allows to change chemical parameters as a function of the temperature following experimental data to reaction rates as basis. The focus of this work is to simulate DNA damage in the range of 0 to 42 °C as a way to benchmark the biological effect of temperature dependent chemical yields. The interval of temperatures was chosen due to the availability of experimental results at the lowest temperature and the temperature limit used in hyperthermia procedures for radiotherapy (Datta, N. R., & Bodis, S. 2019).

2 Methods

To simulate the radiolysis of water, three distinct stages defined by their time duration with respect to each particle traversing the irradiated volume are considered. The first is the physical stage which begins from the incidence of radiation to about 10^{-15} s. In this stage, the radiation traversing the aqueous environment excites water molecules (H_2O^*) or ionizes them (H_2O^+) through energy transfer events to the medium. Subsequently, the physico-chemical stage takes place from about 10^{-15} s to 10^{-12} s, where those excited and ionized water molecules dissociate into the so-called primary chemical species (e^-_{aq}, H_2, H•, •OH and H_3O^+). Finally, the chemical stage (from about 10^{-12} s to 10^{-6} s) occurs where the primary chemical species, initially nonhomogenously distributed in the medium, diffuse through the environment following Brownian dynamics reacting with each other, reducing the yield of primary species, and producing secondary chemical species. After 10^{-5} s the cloud of species is sufficiently sparse (homogeneous) so that no further reactions between primary chemical species are likely (Sanguanmith *et al* 2012). The models used by Geant4-DNA and TOPAS-nBio to simulate these three stages have been reported in detail elsewhere (Karamitros *et al* 2011, 2014, Ramos-Méndez *et al* 2018, Schuemann *et al* 2019, Shin *et al* 2019a, Ramos-Méndez *et al* 2020a, 2021).

2.1 Physics processes and models.

The simulations are performed with a custom-built version of TOPAS-nBio based on the public version beta1.0, which was built on top of TOPAS v3.5. TOPAS-nBio uses a physics module (TsEmDNAPhysics) that includes processes and models to explicitly simulate all interaction events of charged particles in liquid water. The module is based on the Geant4-DNA (v.10.06.p3) constructor option2 described extensively elsewhere (Incerti *et al* 2018a, Shin *et al* 2019a, Ramos-Méndez *et al* 2020a). In brief, the physics list for electron interactions includes the ELSEPA elastic scattering model based on the partial wave theory. For inelastic scattering, the module includes a model based on the formalism of the complex dielectric response function of liquid water considering four ionization shells and five discrete electronic excitation states. The Binary-Encounter-Approximation-with-Exchange model is used to calculate the ionization of the K-shell. Processes for vibrational excitation, electron attachment, and thermalization of sub-excited electrons are also included in the module. This module has been used to validate TOPAS-nBio for water radiolysis of low LET electrons (Ramos-Mendez et al., 2021).

2.2 Chemical parameters as a function of the temperature.

Temperature has several effects on the water radiolysis processes within the three stages mentioned above. In the physical stage, temperature affects the density of water, which in consequence may affect the mean free path of particles traversing it to redistribute the distribution of ionizations and excitations. To account for that change in density, we use a relationship between the density of water and the temperature reported by Elliot and Bartels (2009). For the physico-chemical stage, it is assumed that the dissociation of H_2O^+ and H_2O^* into primary yields is independent of the temperature, as these processes are not thermally activated (Hervé du Penhoat *et al* 2000), thus we used the default dissociation scheme from Geant4-DNA (Shin et al., 2019a). Effects of temperature in the thermalization of sub-excited electrons have been investigated with Monte Carlo by Herve et al (2000). In the work of Hervé du Penhoat, the effect of temperature is simulated by scaling the thermalization distance of the sub-excited electrons considering several temperature-dependent scaling functions. G-values (number of chemical species created or lost per 100 eV of energy deposited) of e^-_{aq} calculated with the scaling functions were reported to only show significant differences with respect to unscaled G-values above 150°C. This temperature value is much higher than that for radiobiology applications including DNA damage in plasmids, used in this work (see below), where temperatures below 50°C have been reported. Therefore, scaling of the thermalization distance was not considered. Nevertheless, for coding verification purposes, the comparison between calculated and existing measured G-values in liquid water ranging from 25°C to 90°C are performed to evaluate the behavior of the model over a broad range of temperatures.

For the simulation of the chemical stage, we rely on the Independent Reaction Times (IRT) method (Tachiya 1983, Clifford *et al* 1986, Green *et al* 1990, Pimblott and Green 1992, Frongillo *et al* 1998, Plante and Devroye 2017). This method has been implemented in TOPAS-nBio (Schuemann *et al* 2019, Ramos-Méndez *et al* 2020) and was validated for water radiolysis and DNA damage at low LET radiation (Ramos-Méndez et al 2021). The IRT implementation is several hundred times faster than the conventional Brownian step-by-step Monte Carlo method available in Geant4-DNA. The chemical parameters (diffusion coefficients and rate constants) in the IRT method are specific for a fixed ambient temperature. Based on the experimental measurements of observed reaction rates compiled by A.J. Elliot and D. Bartels (Elliot 1994, Elliot and Bartels 2009), TOPAS-nBio has been extended to automatically scale the diffusion coefficients and reaction rates as a function of the temperature. The scaling functions and reactions considered in this work are listed in Table 1. Reactions involving the production of HO_2 and O_2^- under low LET radiation contribute negligible to the G-values (<1 %) and thus are not included. Nevertheless, the corresponding reactions must be included in future works considering high-LET radiation. The reference database from Elliot et. al., considers scaling functions for the temperature range between 25°C to 350°C. This temperature range does not cover the lower range 0 °C to 40 °C, for which measured data for plasmid DNA damage have been reported (Tomita *et al* 1995a). Thus, an extrapolation that reflects the expected downwards behavior caused by the reduction of temperature was performed using exponential or power law function fits to the temperature-dependent reaction rate constants between 25°C to 90°C from Elliot and Bartels (2009). This was done considering experimental evidence that damage efficiency of

•OH radicals is reduced at low temperatures (T. Ito et al 1993, Adhikary A. et al 2014). The fitting to Elliot's data to extrapolate the reaction rates for temperatures above 0 °C and below 25 °C for the radiolysis of liquid water is a first approach to simulate the effect of low temperatures on the radiochemistry that affects the DNA damage by low LET irradiation. The type of function and fitting parameters covering the range 0 °C to 90 °C are shown in Table 1; plots for the fitted functions of the reaction rates are shown on Figure 1. The IRT implementation of TOPAS-nBio considers activation control of the reaction rate constant for several reactions. For these reactions, the rate constants shown in Table 1 are used to calculate internally the activation reaction rates as described in detail elsewhere (Ramos-Méndez *et al* 2020a). Finally, for the diffusion coefficients of the chemical species at temperatures other than the ambient temperature, fits to measured data for H_2O, OH^-, H_3O^+ and e_{aq}^- are used, whereas self-diffusion of water is used to scale the coefficients for all the other species. The corresponding functions obtained from (Elliot and Bartels 2009) are shown in Table 2 and presented in Figure 2 as a function of the temperature.

2.3 Verification of G-values for fast electrons in liquid water.

To verify the implementation of temperature-dependent chemical parameters, we compared the G-value of •OH, $e^-_{aq}$and H_2O_2 calculated in water with experimental data from the literature over the temperature range of 25°C to 90°C. The simulation setup consisted of a cube of liquid water of 5 × 5 × 5 cm^3, with an isotropic source of monoenergetic electrons of 1 MeV positioned at the center. The transport of the primary electrons was terminated after an accumulated energy loss of 10 keV was achieved, whereas secondary electrons were not stopped but instead simulated until they thermalized. This setup was adopted in the past to simulate G-values to compare Monte Carlo calculations with experimental data for fast electrons (Pimblott and LaVerne 1997, Uehara and Nikjoo 2006, Ramos-Méndez *et al* 2018, Shin *et al* 2019a), and more recently for the validation of TOPAS-nBio (Ramos-Mendez et al 2021). The total number of simulated histories was 5000 and the G-values at 1 μs (the end of the nonhomogeneous distribution) were presented as a function of temperature. The statistical uncertainties (one standard deviation) were below 1%, one standard deviation. The consistency of the simulations was verified using the balance equation:

$$\begin{aligned} G_{red} &= G(e^-_{aq}) + G(H^\bullet) + 2G(H_2) \\ G_{ox} &= G(\ ^\bullet OH\ ) + 2G(H_2O_2) \\ G_{red} &= G_{ox} \end{aligned} \tag{1}$$

2.4 Simulation of DNA damage as a function of the temperature.

Simulations of DNA damages induced by irradiating supercoiled plasmid DNA geometries with gamma-rays produced by cobalt-60 were performed. Details of the methodology to simulate DNA damage in plasmids dissolved in buffered solutions and irradiated with gamma-rays at ambient temperature using the IRT method are presented elsewhere (Perry *et al* 2021, Ramos-Mendez et al 2021, Dominguez-Kondo et al 2021). For this work, nine plasmids pUC19 (2686 base pairs length) were placed randomly in a spherical phantom of 1.23 μm diameter centered in a cubic phantom of 2 μm side length, the geometrical setup used is presented on Figure 3. The plasmids used in the simulations were pre-generated

using Brownian dynamics following the methodology described in (Ermak and McCammon, 1978; Huang et al, 2001, Ramos-Méndez 2021). Multiple copies of a single plasmid were used, by randomly rotating and placing each copy in the water sphere phantom, the plasmid super helix density was σ=−0.06. The DNA concentration in the sphere matched the experimental concentration of 29.75 μg/mL so the simulation is representative of the experimental irradiation conditions. During the TOPAS-nBio simulations, the plasmids were static following a crystal structure during both the physical and chemical stages.

The sphere and cube were made of an aerated solution consisting of buffered liquid water (density 1 g cm^{-3}) with 1 mM of EDTA, 0.1 mM Tris with 0.27 mM of oxygen added. The concentrations of these scavengers are low enough to neglect any dissociation effect of such molecules to the final SSB and DSB yields. The solution was simulated by including in the simulations the effective •OH scavenging capacity from both scavengers ($s_{eff} = s_{EDTA} + s_{Tris} = 1.62 \times 10^6\ s^{-1}$). Cellular environments are known to have a high •OH, H• and e_{aq}^- scavenger capacity, similar to that at 1 M concentrations of EDTA and TRIS (Klimczak et al 1993, Milligan et al 1993). In the presence of complex scavenging media, like those containing organic molecules, the likelihood of reactions between DNA and radiolitic species may change. Handling the presence of different scavenging media is a capability added to our software. Initial studies of yields of •OH, H• and e_{aq}^- at different scavenger media have been conducted in our previous work (D-Kondo et al., 2021; Ramos-Méndez et al., 2021). These simulation conditions reproduced the experimental setup reported by Tomita et al. (Tomita *et al* 1995a) at ambient temperature, where the measured data for this work was obtained.

For temperature-dependent DNA damage simulations, the following assumptions were made for the realization of reactions between radical species •OH, H•, e^-_{aq} and DNA. The supercoiled DNA conformation was assumed to be unaffected by the temperature; hence the same plasmid geometry model was used for all irradiation doses and temperatures considered. The reactions between chemical species and DNA were set to be controlled by diffusion (Udovičić *et al* 1994). To the best of our knowledge, no temperature-dependent reaction rate constants for reactions between DNA and chemical species have been reported. Hence, room temperature rate constants were used. For the reaction •OH+DNA, the reaction rate constant corresponding to the scavenging capacity *s*eff at room temperature was 8.34 $\times 10^8\ M^{-1}s^{-1}$ as obtained from (Milligan *et al* 1996). For e^-_{aq} and H•, the reaction rate constants at room temperature were obtained from (Buxton *et al* 1988) and are shown in Table 3. In our Monte Carlo model, only reactions between radiolytic species •OH, H• and DNA led to an SSB with a specific efficiency. These efficiency values for TOPAS-nBio simulations were obtained previously as 24% and 0.5% for •OH and H•, respectively (Ramos-Mendez et al 2021). The reported SSBs are taken as Relaxation Events (RE) following the procedure described on Edel et al 2006: RE correspond to a single SSB, an SSB+ or 2 SSB, and linearization events (LE) corresponding to one DSB, and one or more SSB (this is: DSB+, DSB++, etc. following the classification from Terrissol et al., 2004). This procedure was adopted because using every individual lesion in the simulation resulted in a higher number of SSBs (nearly twice as much) than the experimental data from Tomita et al (1995a). By using REs on our simulation as an equivalent to the SSB, the simulated results were on the vicinity of the experimental data and best represent the original

methodology described by Tomita et al. (1995a). To be counted as a DSB, a maximum distance of 10 base pairs between two SSBs on opposite DNA strands was required.

Particle histories were generated uniformly within the limits of the cubic phantom until a specified absorbed dose in the inner sphere was achieved. The dose values ranged from 6.5 Gy to 100 Gy (Tomita et al., 1995a) for temperatures between 0 °C to 42°C. Each primary history consisted of an electron emitted in an isotropic direction. The initial kinetic energy was obtained in a separate simulation using a condensed-history Monte Carlo with TOPAS. For that, Cobalt-60 gamma-rays (two gammas of 1.17 MeV and 1.25 MeV) were simulated irradiating a water phantom cube of 10 cm side length. At 5 cm depth, the spectrum of secondary electrons (Figure 4) set in motion by the gamma-rays was retrieved via phase space. The details of this methodology were previously reported in (Perry *et al* 2021, Ramos-Mendez et al 2021).

3. Results.

3.1 G-values in liquid water for fast electrons

Figure 5 shows the temperature dependent G-values for •OH (top left), e^-_{aq} (top right), and H_2O_2 (bottom left), retrieved at 1 μs after the incidence of radiation. In all these panels, the simulated G-values agree with the measured data for the temperature ranges considered. In the bottom right of the figure, the ratio between yields of oxidative to reductive species (equation 1) is shown. As depicted, the balance material equation was fulfilled within 0.5%, deviation from zero is due to truncation of decimal places.

3.2 DNA damage as a function of the temperature

In Figure 6, the dose dependent SSB and DSB yields for two temperatures are shown. TOPAS-nBio results reproduced the behavior of the measured data for both SSB and DSB curves. In Figure 7, the temperature dependent G-value for SSB, DSB and SSB/DSB ratio at 50 Gy absorbed dose with the available measured data from Tomita et al. (1995a) are shown. The calculated data shows a linear response with the temperature at a rate of (3.16±0.11) x 10^{-10} $Gy^{-1}Da^{-1}$ $°C^{-1}$ (R^2=0.99), (0.13±0.01) x 10^{-10} $Gy^{-1}Da^{-1}$ $°C^{-1}$ (R^2=0.99) and (−0.12±0.04) $°C^{-1}$ (R^2=0.79) for SSB, DSB and SSB/DSB yields, respectively. When comparing to experimental data from other authors that used plasmids of different size, normalization by the weight of the plasmid (measured on Dalton) following the method described on Charlton D E et al. (1989) was made in order to mitigate discrepancies due to differences in the weight and length of the different plasmids.

4 Discussion

Current MCTS codes aim to model DNA damage induction from the initial physics interactions to biological endpoints. Physico-chemical and chemical processes bridge the time between physics interactions and the onset of biological repair processes. In most scenarios, including *in vivo* cells, chemical processes are responsible for the majority of DNA damage (~80%). However, so far MCTS codes typically do not consider temperature as a variable when comparing simulation results to experimental results. This shortcoming

can result in greatly misleading parameter fits and predictions when analyzing data from different experiments.

The measured data used for the scaling of the chemical parameters as a function of temperature (25°C to 90°C) are reported in the presence of scavengers. The comparison between measured data and calculated data in liquid water show agreement. Nevertheless, a comprehensive validation of Monte Carlo simulations must include the presence of scavengers at experimental concentrations to establish a more stringent comparison. We previously demonstrate the capability of TOPAS-nBio to simulate scavenger behavior that reproduced measured hydrogen and hydrogen peroxide G values at room temperature (Ramos-Mendez, et al., 2021).

The temperature at which radiobiological experiments are conducted can have a large impact on the observed outcome. One factor that is typically considered for biological outcome is, whether a cell can initiate DNA repair and proliferation. However, as shown in Figures 2 and 3, temperature can also have a significant impact on the initial DNA damage induction, and thus the resulting DNA repair processes and endpoints. DSB yields between near solid water (0 °C) and proliferating (>36 °C) DNA differ by a factor of 2. Elmroth et al., reported a linearly increasing response of DSB with the temperature using MCF-7 cells suspended in PBS, with a difference factor of 3.4 for the range 2 °C – 42 °C (Elmroth et al., 2000). Consistent with the upward trend from the experimental data, our simulation results shown that DSB grows linearly (R^2=0.99) with increasing temperature as show in Figure 7.

We used relaxation events to represent the SSB lesion in our simulations following Edel's procedure which led the simulated SSBs yields comparable with Tomita's experimental results. This procedure works because individual and complex lesions (SSB, SSBb, SSB+, etc.) are not directly distinguishable in experiments, instead SSB and DSB number need to be deduced from the measure of detectable fractions of supercoiled, circular and linear forms of plasmids using gel electrophoresis [(Edel et al 2006, Vyšín, L., et al (2015)]. On the other hand, DSB are formed from clustered lesions in the DNA strands. On the low LET regime these clustered lesions are rare; this fact explains the low number of DSB compared to SSB on our simulations (around 5%) supported on the results from Vyšín, L et al (2015). We found out that taking either the total individual DSBs simulated or the linearization events to represent DSBs didn't make a difference when comparing them to the experimental data. This also is a result of using low LET radiation since complex lesions that result in LE also increase with LET.

In this work, a geometrical model of pUC19 plasmids generated at a temperature of 20 °C was used for all different temperature sets. This invariance was invoked because only small differences in stand break yields have been observed for different super helix densities (Milligan, 1993; D-Kondo, 2021). Super helix density is used to measure plasmid super coiling, which is affected by temperature and the composition of the solution. A difference of around 5% (D-Kondo et al., 2021) is expected due to plasmid super helix density alone, well within the statistical uncertainties achieved in this work.

In this study, we have demonstrated the importance of considering the temperature of cells or solutions when simulating physico-chemical reactions. We further implemented this functionality in the TOPAS-nBio simulation toolkit and the additional functions described here will become available open source. We anticipate that adoption of this methodology will allow for a better prediction of the outcomes of radiobiological experiments. While our results and fits are so far only valid for low LET irradiation modalities, temperature-dependence will be further expanded to include higher LET modalities in future studies. For higher LET, the number of reactions must be expanded in order to properly simulate the radiolysis of pure liquid water (Baba, et al 2021a; Baba, et al 2021b; Herve du Penhoat, et al 2001) and a revision to the water dissociation schemes could be necessary due to the higher contribution of oxygen reactions (Shin et al., 2021). The results obtained from this and past works (D-Kondo et al., 2021; Ramos-Mendez et al., 2021) show that at low LET modalities, there is no need to simulate oxygen related reactions due to the low contribution that this chemical specie gives to the whole chemical yields. Very low energy electron contributions will also be studied following the experimental results from (Alizadeh, E., & Sanche, L. 2012, Gao Y et. Al. 2021). The temperature dependance of chemical parameters at sub-zero temperatures require the use of updated interaction cross sections that consider phase transition of the medium, which may be the subject of future work. For higher LET modalities, the assumption that indirect SBs are overwhelmingly predominant is no longer valid, specially at high scavenging capacities like cellular environments (Roots & Okada, 1972). Therefore, a direct to indirect SBs analysis must be considered.

5 Conclusions

A method to simulate radiolysis of water as a function of temperature from 0 °C to 90 °C was implemented in TOPAS-nBio, capable to simulate the upwards trend of the radiation induced DNA damage as temperature rises, agreeing with experimental data within experimental statistical uncertainties. This implementation allows one to simulate the irradiation of an aqueous environment for radiobiological experiments under different temperature conditions of 0 °C to 42 °C, which is within the range of medical interest. Calculated G-values and DNA strand break yields as a function of the temperature reproduced published experimental data reasonably well. This new feature of TOPAS-nBio allows the consideration of temperature, an environmental condition that is often neglected in MCTS simulations. By providing temperature-dependent simulation capabilities within TOPAS-nBio, we hope that many groups will adopt this improved framework when analyzing the effects of chemical reactions at varying temperatures and the effects on observed and simulated radiobiological outcomes.

Acknowledgments

This work was partially supported by NIH/NCI R01 CA187003 (TOPAS-nBio). J.D-K. and O.G-G. are doctoral students from Programa de Doctorado en Ciencias Física Aplicada, Benemérita Universidad Autónoma de Puebla and received fellowship 2019–000002-01NACF-05024 and 2019–000002-01NACF-05144, respectively, from CONACYT, the authors thankfully acknowledge computer resources, technical advice and support provided by Laboratorio Nacional de Supercómputo del Sureste de México (LNS), a member of the CONACYT national laboratories, with project No. 201904102C.

References

Adhikary A, Becker D, Sevilla M (2014) Electron Spin Resonance of Radicals in Irradiated DNA. In: Lund A, Shiotani M (eds) Applications of EPR in Radiation Research Springer, Cham. 10.1007/978-3-319-09216-4_8

Alizadeh E, & Sanche L (2012). Precursors of Solvated Electrons in Radiobiological Physics and Chemistry. Chemical Reviews, 112(11), 5578–5602. doi:10.1021/cr300063r [PubMed: 22724633]

Baba K, Kusumoto T, Okada S, & Ishikawa M (2021a). A simulation-based study on water radiolysis species for 1H+4He2+, and 12C6+ ion beams with multiple ionization using Geant4-DNA. Journal of Applied Physics, 129(24). 10.1063/5.0054665

Baba K, Kusumoto T, Okada S, Ogawara R, Kodaira S, Raffy Q, Barillon R, Ludwig N, Galindo C, Peaupardin P, & Ishikawa M (2021b). Quantitative estimation of track segment yields of water radiolysis species under heavy ions around Bragg peak energies using Geant4-DNA. Scientific Reports, 11(1). 10.1038/s41598-021-81215-6

Bernal MA, Bordage MC, Brown JMC, Davídková M, Delage E, El Bitar Z, Enger SA, Francis Z, Guatelli S, Ivanchenko VN, Karamitros M, Kyriakou I, Maigne L, Meylan S, Murakami K, Okada S, Payno H, Perrot Y, Petrovic I, Pham QT, Ristic-Fira A, Sasaki T, Štěpán V, Tran HN, Villagrasa C and Incerti S 2015 Track structure modeling in liquid water: A review of the Geant4-DNA very low energy extension of the Geant4 Monte Carlo simulation toolkit. Physica medica : PM : an international journal devoted to the applications of physics to medicine and biology : official journal of the Italian Association of Biomedical Physics (AIFB) 31 861–74

Boscolo D, Krämer M, Durante M, Fuss MC and Scifoni E 2018 TRAX-CHEM: A pre-chemical and chemical stage extension of the particle track structure code TRAX in water targets Chemical Physics Letters 698 11–8

Buxton GV, Greenstock CL, Helman WP and Ross AB 1988 Critical Review of rate constants for reactions of hydrated electrons, hydrogen atoms and hydroxyl radicals in Aqueous Solution Journal of Physical and Chemical Reference Data 17 513–886

Charlton DE 1986 The range of high LET effects from 125I decays. Radiation Research, 107 163–171 [PubMed: 3749454]

Charlton DE, Nikjoo H and Humm JL 1989 Calculation of Initial Yields of Single- and Double-strand Breaks in Cell Nuclei from Electrons, Protons and Alpha Particles International Journal of Radiation Biology 56 1–19 [PubMed: 2569005]

Clifford P, Green NJB, Oldfield MJ, Pilling MJ and Pimblott SM 1986 Stochastic Models of Multi-species Kinetics in Radiation-induced Spurs J. Chem. Soc., Faraday Trans. 1 82 2673–89

Datta NR, & Bodis S (2019). Hyperthermia with radiotherapy reduces tumour alpha/beta: Insights from trials of thermoradiotherapy vs radiotherapy alone. Radiotherapy and oncology: journal of the European Society for Therapeutic Radiology and Oncology, 138, 1–8. 10.1016/j.radonc.2019.05.002 [PubMed: 31132683]

Dingfelder M, Ritchie RH, Turner JE, Friedland W, Paretzke HG and Hamm RN 2008 Comparisons of Calculations with PARTRAC and NOREC: Transport of Electrons in Liquid Water Radiation Research 169 584–94 [PubMed: 18439039]

Domínguez-Kondo J, Moreno E, Stepan V, Stefanová K, Perrot Y, Villagrasa C, Incerti S, De Celis Alonso B, Schuemann J, Faddegon B and Ramos J 2021 DNA damage modeled with Geant4-DNA: effects of plasmid DNA conformation and experimental conditions. Physics in Medicine and Biology 10.1088/1361-6560/ac3a22.

Edel S, Terrissol M, Peudon A, Kümmerle E, & Pomplun E (2006). Computer simulation of strand break yields in plasmid pBR322: DNA damage following 125I decay. Radiation Protection Dosimetry, 122(1–4), 136–140. 10.1093/rpd/ncl453 [PubMed: 17185311]

Elliot AJ and Bartels D 2009 The reaction Set, rate constants and g-values for the simulation of the radiolysis of light water Atomic Energy of Canada Limited Report 153–127160

Elliot AJ 1994 Rate constants and G-values for the simulation of the radiolysis of light water over the range 0–300 C vol AECL-11073 (Canada: AECL)

Elliot AJ, Chenier MP and Ouellette DC (1993) “Temperature Dependence of g Values for H2O and D2O Irradiated with Low Linear Energy Transfer Radiation.” J. Chem. Soc. Faraday Trans Vol. 89, pp. 1193–1197.

Elmroth K, Nygren J, Erkell LJ and Hultborn R 2000 Radiation-induced double-strand breaks in mammalian DNA: Influence of temperature and DMSO International Journal of Radiation Biology 76 1501–8 [PubMed: 11098853]

Ermak DL and McCammon JA 1978 Brownian dynamics with hydrodynamic interactionsJ. Chem. Phys 69 1352–60

Figueroa-González G and Pérez-Plasencia C 2017 Strategies for the evaluation of DNA damage and repair mechanisms in cancer Oncol. Lett 13 3982–8 [PubMed: 28588692]

Friedland W, Schmitt E, Kundrát P, Dingfelder M, Baiocco G, Barbieri S and Ottolenghi A 2017 Comprehensive track-structure based evaluation of DNA damage by light ions from radiotherapy-relevant energies down to stopping Scientific Reports 7 45161 [PubMed: 28345622]

Frongillo Y, Goulet T, Fraser M-J, Cobut V, Patau JP and Jay-Gerin J-P 1998 Monte Carlo Simulation of Fast Electron And Proton Tracks In Liquid Water - II. Nonhomogeneous Chemistry Radiation Physics and Chemistry 51 245–54

Gao Y, Zheng Y, Sanche L. (2021) Low-Energy Electron Damage to Condensed-Phase DNA and Its Constituents. International Journal of Molecular Sciences 22. DOI:10.3390/ijms22157879

Green NJB, Pilling MJ and Clifford P 1990 Stochastic Modeling of Fast Kinetics in a Radiation Track Society 94 251–8

Hervé du Penhoat M-A, Goulet T, Frongillo Y, Fraser M-J, Bernat P and Jay-Gerin J-P 2000 Radiolysis of Liquid Water at Temperatures up to 300 C: A Monte Carlo Simulation Study The Journal of Physical Chemistry A 104 11757–70

Hervé du Penhoat M-A, Meesungnoen J, Goulet T, Filali-Mouhim A, Mankhetkorn S and Jay-Gerin J-P 2001 Linear-energy-transfer effects on the radiolysis of liquid water at temperatures up to 300°C – a Monte-Carlo study Chemical Physics Letters 341 135–43

Huang J, Schlick T, & Vologodskii A (2001). Dynamics of site juxtaposition in supercoiled DNA. Proceedings of the National Academy of Sciences of the United States of America, 98(3), 968–973. 10.1073/pnas.98.3.968 [PubMed: 11158579]

Incerti S, Baldacchino G, Bernal M, Capra R, Champion C, Francis Z, GuÈye P, Mantero A, Mascialino B, Moretto P, Nieminen P, Villagrasa C and Zacharatou C 2010a THE Geant4-DNA project International Journal of Modeling, Simulation, and Scientific Computing 1 157–78

Incerti S, Ivanchenko A, Karamitros M, Mantero A, Moretto P, Tran HN, Mascialino B, Champion C, Ivanchenko VN, Bernal M a, Francis Z, Villagrasa C, Baldacchin G, Guèye P, Capra R, Nieminen P and Zacharatou C 2010b Comparison of GEANT4 very low energy cross section models with experimental data in water. Medical physics 37 4692–708 [PubMed: 20964188]

Incerti S, Kyriakou I, Bernal MA, Bordage MC, Francis Z, Guatelli S, Ivanchenko V, Karamitros M, Lampe N, Lee SB, Meylan S, Min CH, Shin WG, Nieminen P, Sakata D, Tang N, Villagrasa C, Tran HN and Brown JMC 2018a Geant4-DNA example applications for track structure simulations in liquid water: A report from the Geant4-DNA Project Medical Physics 45 e722–39

Ito T, Baker SC, Stickley CD, Peak JG, & Peak MJ (1993). Dependence of the yield of strand breaks induced by gamma-rays in DNA on the physical conditions of exposure: water content and temperature. International journal of radiation biology, 63(3), 289–296. 10.1080/09553009314550391 [PubMed: 8095278]

Janik D, Janik I, and Bartels DM (2007) “Neutron and β/γ Radiolysis of Water up to Supercritical Conditions. 1. β/γ Yields for H2, H. Atom, and Hydrated Electron.” J. Phys. Chem. A Vol. 111, pp. 7777–7786. [PubMed: 17645317]

Jha KN, Ryan TG and Freeman GR (1972) “Radiolysis of H2O and D2O between 0 and 300°.” J. Phys. Chem Vol. 79, pp. 868–870.

Jones GDD, Boswell TV and Ward JF 1994 Effects of postirradiation temperature on the yields of radiation-induced single- and double-strand breakage in SV40 DNA Radiation Research 138 291–6 [PubMed: 8184001]

Kanike V, Meesungnoen J, Sanguanmith S, Guzonas DA, Stuart CR and Jay-Gerin J-P 2016 GENERATION OF ULTRAFAST TRANSIENT ACID SPIKES IN HIGH-TEMPERATURE

WATER IRRADIATED WITH LOW LINEAR ENERGY TRANSFER RADIATION CNL Nuclear Review 1–10

Karamitros M, Luan S, Bernal MA, Allison J, Baldacchino G, Davidkova M, Francis Z, Friedland W, Ivantchenko V, Ivantchenko A, Mantero A, Nieminem P, Santin G, Tran HN, Stepan V and Incerti S 2014 Diffusion-controlled reactions modeling in Geant4-DNA Journal of Computational Physics 274 841–82

Karamitros M, Mantero A, Incerti S, Friedland W, Baldacchino G, Barberet P, Bernal M, Capra R, Champion C, El Bitar Z, Francis Z, Gueye P, Ivanchenko A, Ivanchenko V, Kurashige H, Mascialino B, Moretto P, Nieminen P, Santin G, Seznec H, Tran HN, Villagrasa C and Zacharatou C 2011 Modeling Radiation Chemistry in the Geant4 Toolkit Progress in Nuclear Science and Technology 2 503–8

Kassis A, Harapanhalli R, & Adelstein S (1999). Comparison of Strand Breaks in Plasmid DNA after Positional Changes of Auger Electron-Emitting Iodine-125. Radiation research, 152(5), 530–538. [PubMed: 10521930]

Kent MC and Sims HE (1992) "The Yield of g-Radiolysis Products from Water at Temperatures up to 270°C." Harwell Report AEA-RS-2301

Klimczak U, Ludwig DC, Mark F, Rettberg P and Schulte-Frohlinde D 1993 Irradiation of plasmid and phage DNA in water-alcoholmixtures: Strand breaks and lethal damage as a function of scavenger concentration Int. J. Radiat. Biol 64 497–510 [PubMed: 7902389]

Lampe N, Karamitros M, Breton V, Brown JMC, Sakata D, Sarramia D and Incerti S 2018 Mechanistic DNA damage simulations in Geant4-DNA Part 2: Electron and proton damage in a bacterial cell Physica Medica 48 146–55 [PubMed: 29371062]

Milligan JR, Aguilera JA and Ward JF 1993 Variation of single-strand break yield with scavenger concentration for plasmid DNA irradiated in aqueous solution Radiat. Res 133 151–7 [PubMed: 8382368]

Milligan JR, Wu CCL, Ng JYY, Aguilera JA and Ward JF 1996 Characterization of the reaction rate coefficient of DNA with the hydroxyl radical Radiation research 146 510–3 [PubMed: 8896577]

Moiseenko VV, Hamm RN, Waker AJ and Prestwich WV 1998 Modelling DNA damage induced by different energy photons and tritium beta-particles International Journal of Radiation Biology 74 533–50 [PubMed: 9848272]

Nikjoo H, Emfietzoglou D, Liamsuwan T, Taleei R, Liljequist D and Uehara S 2016 Radiation track, DNA damage and response—a review Reports on Progress in Physics 79 116601 [PubMed: 27652826]

Perry CC, Ramos-Méndez J and Milligan JR 2021 Boronated Condensed DNA as a Heterochromatic Radiation Target Model Biomacromolecules acs.biomac.1c00106

Pimblott SM and Green NJB 1992 Stochastic modeling of partially diffusion-controlled reactions in spur kinetics Journal of Physical Chemistry 96 9338–48

Pimblott SM and LaVerne JA 1997 Stochastic Simulation of the Electron Radiolysis of Water and Aqueous Solutions The Journal of Physical Chemistry A 101 5828–38

Plante I 2011 A Monte-Carlo step-by-step simulation code of the non-homogeneous chemistry of the radiolysis of water and aqueous solutions-Part II: Calculation of radiolytic yields under different conditions of LET, pH, and temperature Radiation and Environmental Biophysics 50 405–15 [PubMed: 21594646]

Plante I and Devroye L 2017 Considerations for the independent reaction times and step-by-step methods for radiation chemistry simulations Radiation Physics and Chemistry 139 157–72

Ramos-Méndez J, Domínguez-Kondo N, Schuemann J, McNamara A, Moreno-Barbosa E and Bruce Faddegon 2020 LET-Dependent Intertrack Yields in Proton Irradiation at Ultra-High Dose Rates Relevant for FLASH Therapy Radiation Research 194 5–7

Ramos-Mendez JA, LaVerne JA, Domínguez-Kondo JN, Milligan J, Stepan V, Stefanová K, Perrot Y, Villagrasa C, Shin W-G, Incerti S, McNamara AL, Paganetti H, Perl J, Schuemann J, & Faddegon BA (2021). TOPAS-nBio validation for simulating water radiolysis and DNA damage under low-LET irradiation. Physics in Medicine & Biology, 66(June), 1–12. 10.1088/1361-6560/ac1f39

Ramos-Méndez J, Perl J, Schuemann J, McNamara A, Paganetti H and Faddegon B 2018 Monte Carlo simulation of chemistry following radiolysis with TOPAS-nBio Physics in Medicine & Biology 63 105014 [PubMed: 29697057]

Ramos-Méndez J, Shin W, Karamitros M, Domínguez-Kondo J, Tran NH, Incerti S, Villagrasa C, Perrot Y, Štěpán V, Okada S, Moreno-Barbosa E and Faddegon B 2020a Independent reaction times method in Geant4-DNA: Implementation and performance Medical Physics 47 5919–30 [PubMed: 32970844]

Roots R, & Okada S (1972). Protection of DNA molecules of cultured mammalian cells from radiation-induced single-Strand scissions by various alcohols and SH compounds. International Journal of Radiation Biology, 21(4), 329–342. 10.1080/09553007214550401

Sahu SK, Kortylewicz ZP, Baranowska-Kortylewicz J, Taube RA, Adelstein SJ and Kassis AI 1997 Strand Breaks after the Decay of Iodine-125 in Proximity to Plasmid pBR322 DNA Radiation Research 147 401 [PubMed: 9092918]

Sakata D, Lampe N, Karamitros M, Kyriakou I, Belov O, Bernal MA, Bolst D, Bordage M-CC, Breton V, Brown JMC, Francis Z, Ivanchenko V, Meylan S, Murakami K, Okada S, Petrovic I, Ristic-Fira A, Santin G, Sarramia D, Sasaki T, Shin W-GG, Tang N, Tran HN, Villagrasa C, Emfietzoglou D, Nieminen P, Guatelli S and Incerti S 2019 Evaluation of early radiation DNA damage in a fractal cell nucleus model using Geant4-DNA Physica Medica 62 152–7 [PubMed: 31109825]

Sanguanmith S, Meesungnoen J, Muroya Y, Lin M, Katsumura Y and Jay-Gerin JP 2012 On the spur lifetime and its temperature dependence in the low linear energy transfer radiolysis of water Physical Chemistry Chemical Physics 14 16731–6 [PubMed: 23138332]

Schmidt KH; Han P; Bartels DM TemperatureDependence of Solvated Electron-Diffusion in H2O and D2O. J. Phys. Chem 1992, 96, 199–206

Schuemann J, McNamara AL, Ramos-Méndez J, Perl J, Held KD, Paganetti H, Incerti S and Faddegon B 2019 TOPAS-nBio: An Extension to the TOPAS Simulation Toolkit for Cellular and Sub-cellular Radiobiology Radiation Research 191 125 [PubMed: 30609382]

Shin W-G, Ramos-Mendez J, Faddegon B, Tran HN, Villagrasa C, Perrot Y, Okada S, Karamitros M, Emfietzoglou D, Kyriakou I, Bordage MC, Sakata D, Guatelli S, Choi HJ, Min CH, Lee SB and Incerti S 2019a Evaluation of the influence of physical and chemical parameters on water radiolysis simulations under MeV electron irradiation using Geant4-DNA Journal of Applied Physics 126 114301

Shin WG, Ramos-Mendez J, Tran NH, Okada S, Perrot Y, Villagrasa C, & Incerti S (2021). Geant4-DNA simulation of the pre-chemical stage of water radiolysis and its impact on initial radiochemical yields. Physica Medica, 88, 86–90. 10.1016/j.ejmp.2021.05.029 [PubMed: 34198026]

Spinks JWT and Woods RJ (1990) “An Introduction to Radiation Chemistry” Publisher: John Wiley & Sons, Inc., Third Edition.

Sultana A, Meesungnoen J and Jay-Gerin JP 2020 Yields of primary species in the low-linear energy transfer radiolysis of water in the temperature range of 25–700 °c Physical Chemistry Chemical Physics 22 7430–9 [PubMed: 32215415]

Stefanic I and LaVerne JA (2002) “Temperature Dependence of the Hydrogen Peroxide Production in the g-Radiolysis of Water.” J. Phys. Chem. A Vol. 106, pp. 447–452.

Štěpán V and Davídková M 2014 RADAMOL tool: Role of radiation quality and charge transfer in damage distribution along DNA oligomer Guest editors: Andrey V. Solov’yov, Nigel Mason, Paulo Limão-Vieira, Malgorzata Smialek-Telega European Physical Journal D 68

Tachiya M 1983 Theory of diffusion-controlled reactions: Formulation of the bulk reaction rate in terms of the pair probability Radiation Physics and Chemistry (1977) 21 167–75

Terrissol M, Edel S, & Pomplun E (2004). Computer evaluation of direct and indirect damage induced by free and DNA-bound Iodine-125 in the chromatin fibre. International Journal of Radiation Biology, 80(11–12), 905–908. doi:10.1080/09553000400017622 [PubMed: 15764400]

Tomita H, Kai M, Kusama T and Aoki Y 1995a Strand Break Formation in Plasmid DNA Irradiated in Aqueous Solution: Effect of Medium Temperature and Hydroxyl Radical Scavenger Concentration. Journal of Radiation Research 36 46–55 [PubMed: 7616487]

Lj Udovičić, Mark F, Bothe E and Udovicic Lj 1994 Yields of Single-Strand Breaks in Double-Stranded Calf Thymus DNA Irradiated in Aqueous Solution in the Presence of Oxygen and Scavengers Radiation Research 140 166 [PubMed: 7938464]

Uehara S and Nikjoo H 2006 Monte Carlo simulation of water radiolysis for low-energy charged particles. Journal of radiation research 47 69–81 [PubMed: 16571920]

Vyšín L, Pachnerová Brabcová K, Štěpán V, Moretto-Capelle P, Bugler B, Legube G, Cafarelli P, Casta R, Champeaux JP, Sence M, Vlk M, Wagner R, Štursa J, Zach V, Incerti S, Juha L, Davídková M (2015). Proton-induced direct and indirect damage of plasmid DNA. Radiation and Environmental Biophysics, 54(3), 343–352. doi:10.1007/s00411-015-0605-6 [PubMed: 26007308]

Zhu H, McNamara AL, McMahon SJ, Ramos-Mendez J, Henthorn NT, Faddegon B, Held KD, Perl J, Li J, Paganetti H and Schuemann J 2020 Cellular Response to Proton Irradiation: A Simulation Study with TOPAS-nBio Radiation Research 194 9 [PubMed: 32401689]

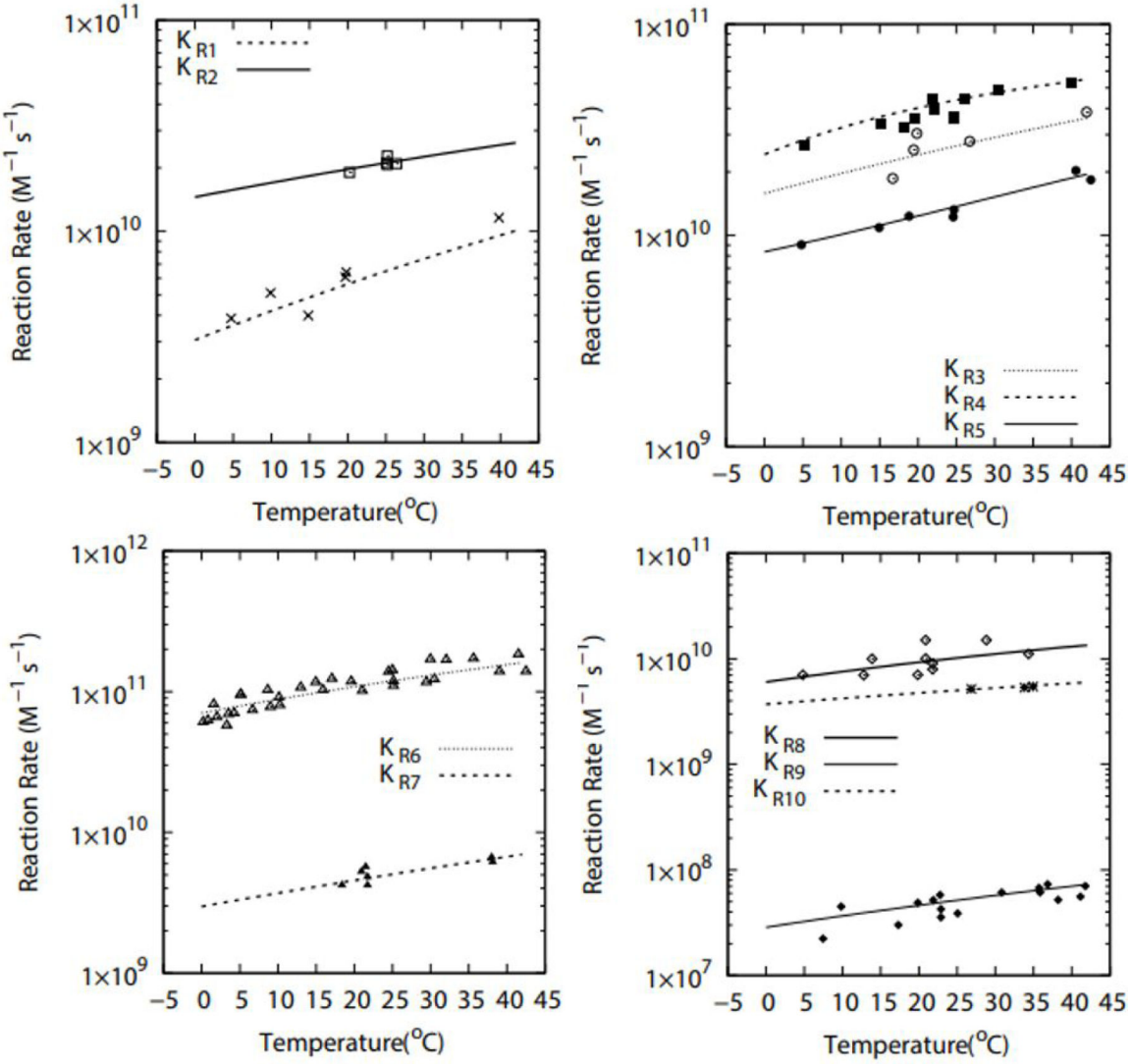

Figure 1:

Plots for the analytical functions dependent on temperature used to scale the rates K_{Ri} of the reactions used in this work compared to experimental data compiled by Elliot & Bartels (2009), for K_{R1} (□), K_{R2}(×), K_{R3}(⊙), K_{R4}(■), K_{R5}(●), K_{R6}(△),K_{R7}(▲)K_{R8}(◇),K_{R9}(◆),K_{R10}(✳)

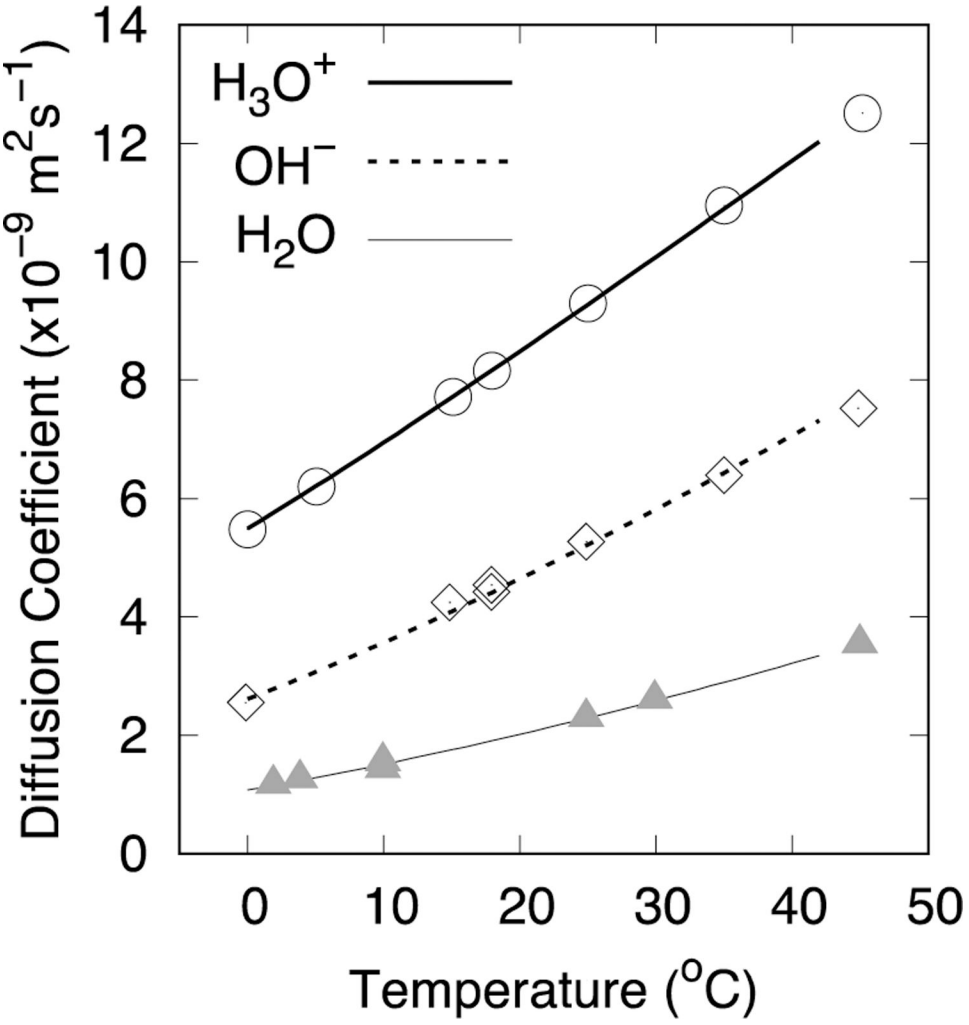

Figure 2:

plots for the polynomials used for calculating diffusion coefficients of H_3O^3 (thick solid line), OH^- (dashed line) and H_2O (thin solid line) as a function of the temperature, the diffusion coefficients for the rest of chemical species are calculated using Self-diffusion of water (Elliot A. J. 1994, Hervé M. A. 2000) Experimental data for H_3O^3 (○), OH^- (◇) and H_2O (▲) were compiled by Elliot & Bartels, 2009.

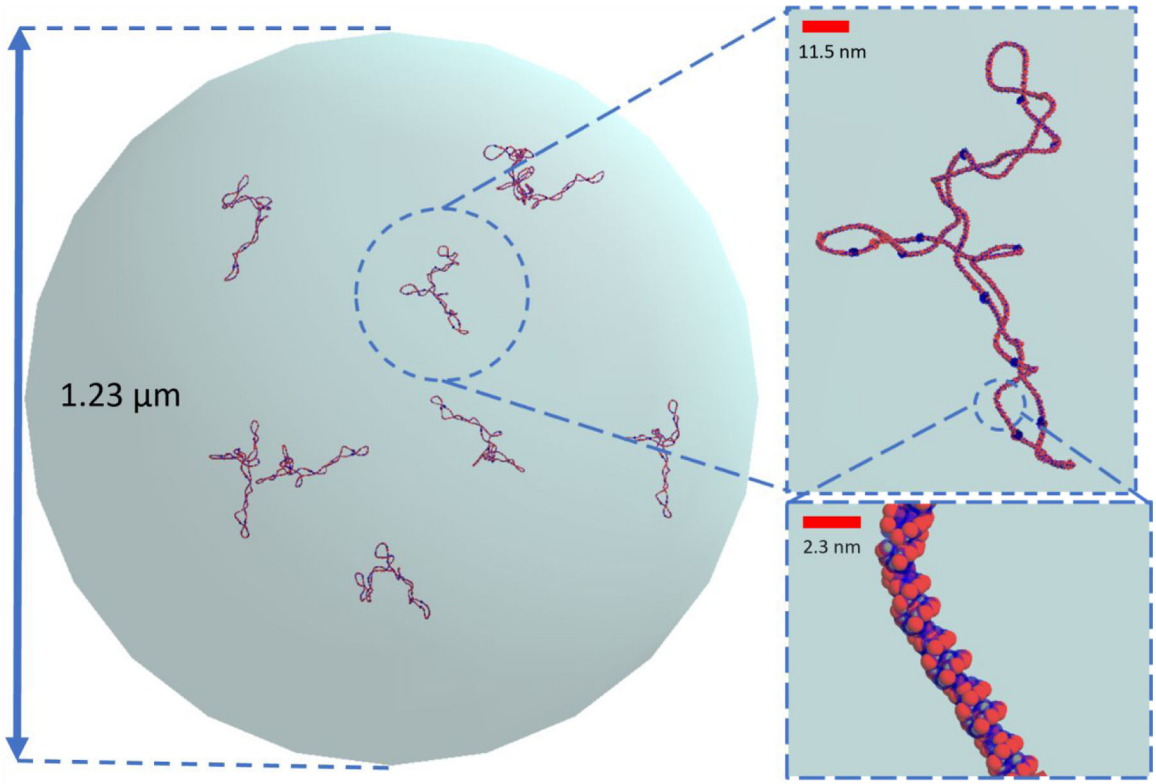

Figure 3:
Plasmids pUC19 (2686 base pairs length) used on this work, the methodology to construct this model is described on Ermak and McCammon 1978, Huang et al 2001. A similar configuration has been used on a previous work (Ramos-Mendez et al 2021).

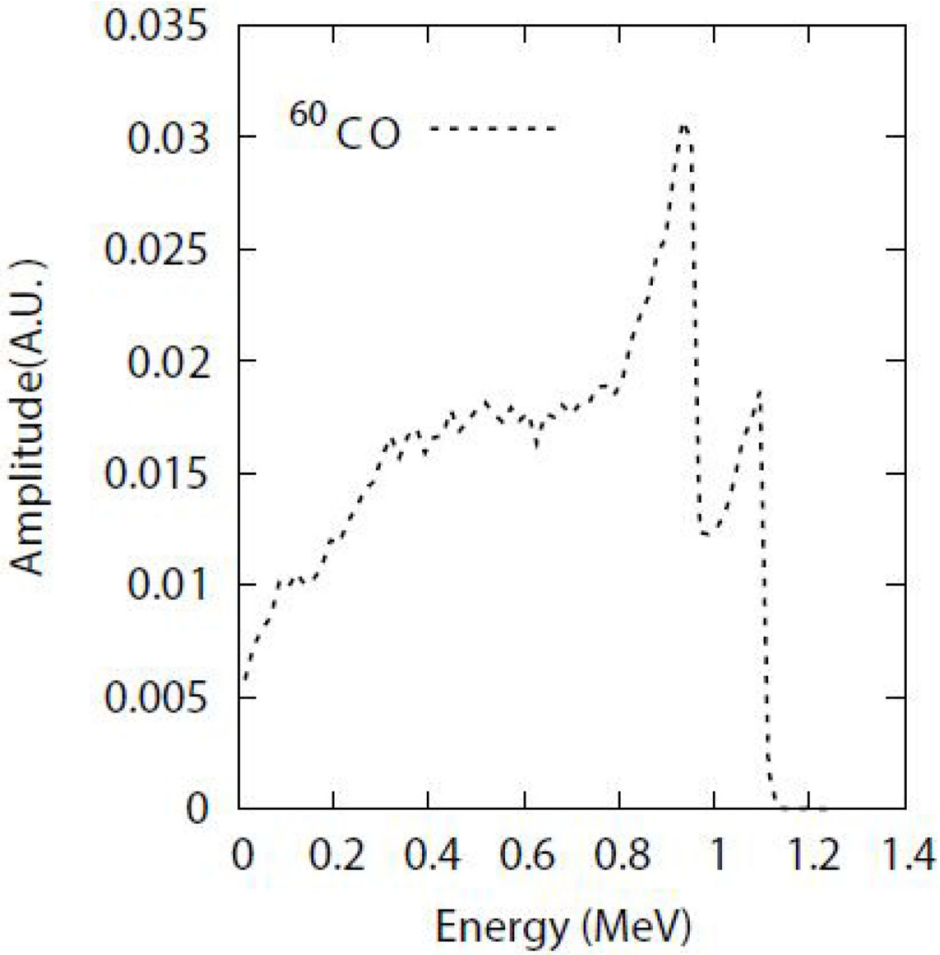

Figure 4.
spectrum of secondary electrons set in motion by the Cobalt-60 gamma-rays, the methodology to obtain this spectrum is reported in (Perry et al 2021, Ramos-Mendez et al 2021).

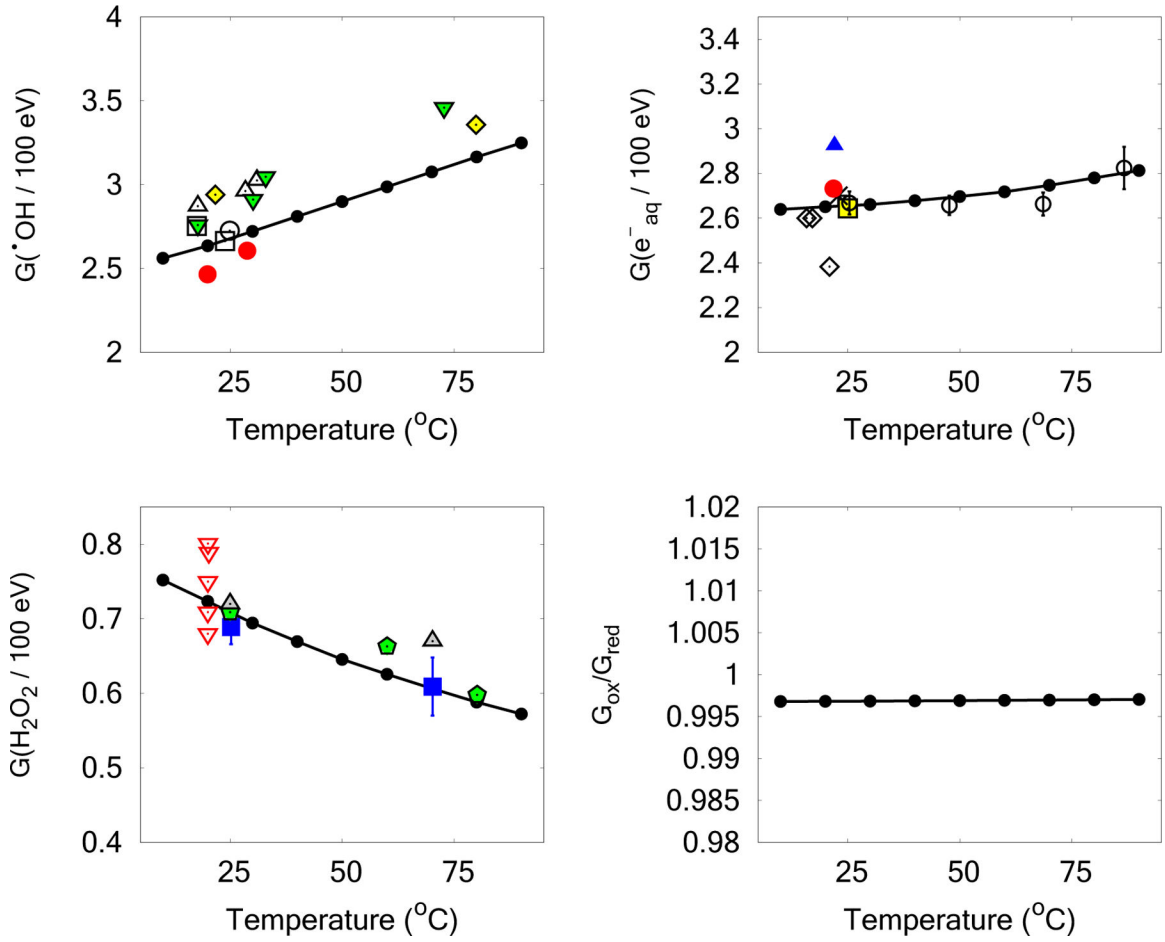

Figure 5:

Temperature dependence of the G-values for •OH (panel a), e^-_{aq} (panel b), and H_2O_2 (panel c). Calculated data is shown with black solid points connected with a solid line. The panel d) shows the ratio between oxidative to reduction species ensuring material balance within 0.5%. Measured data for •OH: Spinks and Woods (1990), empty circles; Elliot et al., (1993) (25 mM HCO_3^-/Air, empty squares), (1 mM Ferrocyanide, diamond), (0.1 M HCO_3^-/O_2 triangles); (0.1 M HCO_3^-/Air, inverted triangles); (60 mM HCO_3^-/Air, filled circles). Measured data for e^-_{aq}: Elliot et al. (1993) (10^{-3} M $NO_3^-/5\times10^{-3}$ M Phosphate ion, square), Schmidt et al (1992) (empty circles); Kent & Sims (1992) (diamonds); Jha et al. (1972) (crosses); Janik et al. (2007) (filled circle); Janik et al (2007) (triangle). Data for H_2O_2 is from Elliot et al. (1993) (squares); Elliot 1994 (10^{-3} m NO_3^- / 10^{-4} m NO_2^- /) (triangles); Kent & Sims (1992) (inverted triangles); Stefanic & LaVerne (2002) (polygons).

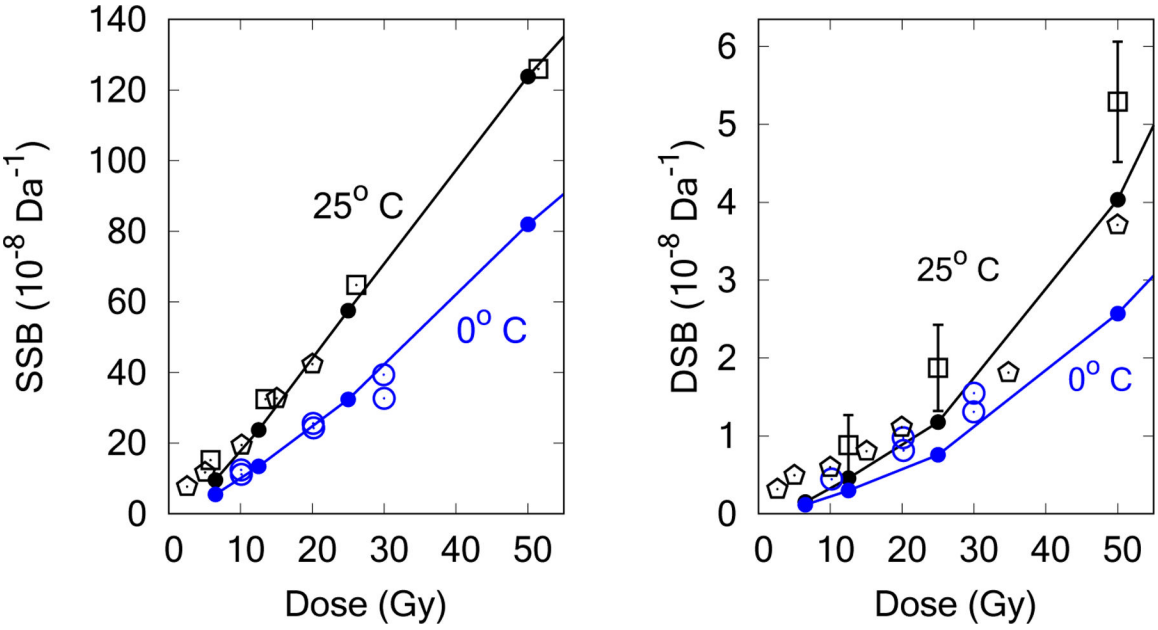

Figure 6:

SSB (left) and DSB (right) yields as a function of the absorbed dose. Monte Carlo data is shown with filled circles connected with solid lines. Experimental data corresponds to plasmids (pUC18 or pBR322) shown with open symbols. The experimental data was obtained from squares (□) Tomita et al (1995a) at 25°C; polygon (▯) Kassis et al (1999) at 25°C; circles (○) Sahu et al (1997) at 0°C.

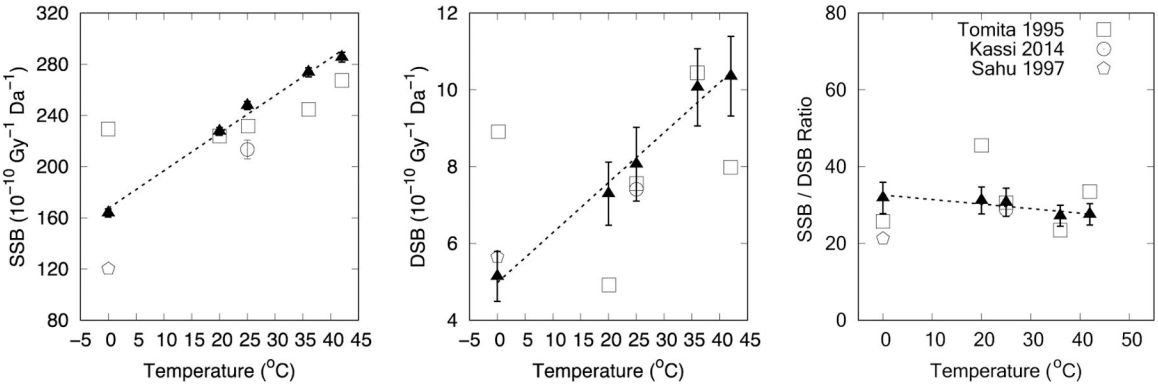

Figure 7:

Temperature dependent SSB (left), DSB (center) and SSB/DSB ratio (right) in supercoiled plasmids for an absorbed dose of 50 Gy. Experimental data from Tomita (1995a) connected squares (□), Kassis et al. (1999) circle (○) and Sahu (1997) polygon (▯) are also shown. Monte Carlo data are shown with filled triangles. The Monte Carlo data set is fitted with a least-mean-square straight line with slope (2.94 ± 0.11) x 10^{-10} $Gy^{-1}Da^{-1}$ °C^{-1} (R^2=0.99), (0.13 ± 0.01) x 10^{-10} $Gy^{-1}Da^{-1}$ °C^{-1} (R^2=0.99) and (−0.12 ±0.04) °C–1 (R^2=0.78) for SSB, DSB and SSB/DSB ratio, respectively. Fits are shown with the dotted lines.

Table 1:

Reaction scheme and functions used for calculating rate constants used in this work as a function of the temperature. T in Kelvin. *R Universal Gas Constant. Oxygen reactions are considered as background reactions, with an initial concentration of $[O_2]$ = 0.27 mM. Oxygen reactions were treated as temperature independent.

Reaction	Analytical functions for temperature between *0 °C to 90 °C*
$e^-_{aq} + e^-_{aq}(+2H_2O) \rightarrow H_2 + 2OH^-$	$k_{R1} = 2.33 \times 10^{13} \exp(-20.3/RT)$
$e^-_{aq} + H_3O^+ \rightarrow H^\bullet + H_2O$	$k_{R2} = 1.24 \times 10^{12} \exp(-10.1/RT)$
$e^-_{aq} + H^\bullet(+H_2O) \rightarrow H_2 + OH^-$	$k_{R3} = 7.52 \times 10^{12} \exp(-14.0/RT)$
$e^-_{aq} + {}^\bullet OH(+H_2O) \rightarrow OH^- + H_2O$	$\text{Log10}(k_{R4}) = -39.29 + 4.597 \times 10^{-1} T - 1.422 \times 10^{-3} T^2 + 1.482 \times 10^{-6} T^3$
$e^-_{aq} + H_2O_2(+H_2O) \rightarrow OH^- + {}^\bullet OH$	$\text{Log10}(k_{R5}) = 19.08 - 1.062 \times 10^{-1} T + 3.804 \times 10^{-4} T^2 - 4.186 \times 10^{-7} T^3$
$H_3O^+ + OH^- \rightarrow 2H_2O$	$\text{Log10}(k_{R6}) = 3.78 + 4.65 \times 10^{-2} T - 9.32 \times 10^{-5} T^2 + 6.48 \times 10^{-8} T^3$
$H^\bullet + H^\bullet \rightarrow H_2$	$\text{Log10}(k_{R7}) = 4.64 + 2.74 \times 10^{-2} T - 4.19 \times 10^{-5} T^2 + 2.33 \times 10^{-8} T^3$
$H^\bullet + {}^\bullet OH \rightarrow H_2O$	$\text{Log10}(k_{R8}) = 5.12 \times 10^{-1} + 6.56 \times 10^{-2} T - 1.46 \times 10^{-4} T^2 + 1.10 \times 10^{-7} T^3$
$H^\bullet + H_2O_2 \rightarrow {}^\bullet OH + H_2O$	$k_{R9} = 3.21 \times 10^{10} \exp(-15.95/RT)$
${}^\bullet OH + {}^\bullet OH \rightarrow H_2O_2$	$\text{Log10}(k_{R10}) = 5.97 + 2.23 \times 10^{-2} T - 3.96 \times 10^{-5} T^2 + 2.27 \times 10^{-8} T^3$
Oxygen reactions	***Reaction rate $K_{obs}(M^{-1}s^{-1})$***
$e^-_{aq} + O_2 \rightarrow O_2^-$	1.90×10^{10}
$H^\bullet + O_2 \rightarrow HO_2$	2.10×10^{10}

Table 2:

Method for calculating diffusion coefficients of chemical species used in this work as a function of the temperature using the work of Elliot (Elliot, 1994) and Hervé (Hervé, 2000). T and t are temperatures in Kelvin and °C respectively.

Molecule	Diffusion coefficient At 25°C (10^{-9} m^2s^{-1})	Method of calculation
H•	7.0	Self-diffusion of water
•OH	2.2	Self-diffusion of water
H_2O_2	2.3	Self-diffusion of water
H_2	4.8	Self-diffusion of water
e^-_{aq}	4.9	Polynomial
H_3O^+	9.4	Polynomial
OH^-	5.3	Polynomial
Polynomials for Molecules (D in units of 10^{-9} m^2 s^{-1})		
D_{H_2O}	$\log D = 4.311 - 2.722\times10^3\,T^{-1} + 8.565\times10^5 T^{-2} - 1.181\times10^8 T^{-3}$	
D_{OH^-}	$\log D = 3.324 - 1.719\times10^3\,T^{-1} + 5.890\times10^5 T^{-2} - 9.188\times10^7 T^{-3}$	
$D_{H_3O^+}$	$\log D = 2.672 - 9.847\times10^2\,T^{-1} + 3.306\times10^5 T^{-2} - 5.621\times10^7 T^{-3}$	
$D_{e^-_{aq}}$	$D = 1.97\times10^{-5} + 1.05\times10^{-6}\,t + 2.11\times10^{-9}\,t^2 + 1.07\times10^{-10}\,t^3$	
Self-diffusion of water for molecule *I* (D in units 10^{-9} m^2 s^{-1})		
D_i	$D_i(25°C)\cdot\frac{D_{H_2O}(t)}{D_{H_2O}(25°C)}$	

Table 3

Reaction coefficients between DNA and chemical species.

Reaction	k_{obs} (/M/s)
•OH + DNA	8.34×10^{8} *
H• + DNA	0.03×10^{9}
e^{-}_{aq} + DNA	0.01×10

*For a scavenging capacity of 1.62×10^{6} s^{-1}, *from* (Milligan et al. 1996)